J. Membrane Biol. 134, 155–167 (1993)

The Journal of
Membrane
Biology

Voltage-Dependent Calcium and Potassium Conductances in Striated Muscle Fibers from the Scorpion, *Centruroides sculpturatus*

Wm. F. Gilly, Todd Scheuer*
Hopkins Marine Station, Stanford University, Pacific Grove, California 93950

Received: 8 October 1992/Revised: 20 January 1993

Abstract. Ionic currents responsible for the action potential in scorpion muscle fibers were characterized using a three-intracellular microelectrode voltage clamp applied at the fiber ends (8–12°C). Large calcium currents (I_{Ca}) trigger contractile activation in physiological saline (5 mM Ca) but can be studied in the absence of contractile activation in a low Ca saline (≤2.5 mM). Barium (Ba) ions (1.5–3 mM) support inward current but not contractile activation.

Ca conductance kinetics are fast (time constant of 3 msec at 0 mV) and very voltage dependent, with steady-state conductance increasing *e*-fold in approximately 4 mV. Half-activation occurs at −25 mV. Neither I_{Ca} nor I_{Ba} show rapid inactivation, but a slow, voltage-dependent inactivation eliminates I_{Ca} at voltages positive to −40 mV. Kinetically, scorpion channels are more similar to L-type Ca channels in vertebrate cardiac muscle than to those in skeletal muscle.

Outward K currents turn on more slowly and with a longer delay than do Ca currents, and K conductance rises less steeply with voltage (*e*-fold change in 10 mV; half-maximal level at 0 mV). K channels are blocked by externally applied tetraethylammonium and 3,4 diaminopyridine.

Key words: Calcium channel — Potassium channel — Arthropod muscle — Voltage clamp

The role of Ca channel proteins in excitation-contraction coupling of vertebrate skeletal and cardiac muscle has long been controversial, but our understanding of this important area has advanced greatly in recent years (Adams & Beam, 1990; Rios, Ma & Gonzalez, 1991). In skeletal muscle the invaginating transverse tubules (TT) provide a pathway for propagation of a Na-mediated action potential. Specialized connections of TT with the sarcoplasmic reticulum (SR) occur at diadic or triadic junctions which are characterized by arrays of specialized "feet" bridging the two membranes (Ferguson, Schwartz & Franzini-Armstrong, 1984). TT membrane is rich in dihydropyridine (DHP) receptor/Ca channel protein, and depolarization of TT membrane results in a "gating current" due to reorientation of charged, intramembranous molecules (Schneider & Chandler, 1973) that have been identified as DHP-receptors (Rios & Brum, 1987; Adams et al., 1990). This charge movement, in turn, controls Ca release by the SR (Schneider, 1981; Pizarro et al., 1991). The molecular basis for coupling charge movement to Ca release remains unknown, although it is clear that specific cytoplasmic portions of the DHP-receptor are critically important (Tanabe et al., 1990).

Although DHP-receptors in skeletal muscle can also function as voltage-controlled, L-type Ca channels (Tanabe et al., 1988), inward Ca current is not essential for normal excitation-contraction (E-C) coupling (McClesky, 1985). This situation contrasts to that in vertebrate cardiac muscle, where inward Ca current, primarily through L-type Ca channels (Bean, 1989), is necessary for contractile activation (Morad, Goldman & Trentham, 1983). Charge movement in cardiac muscle is largely gating current for these Ca channels (Shirokov et al., 1992), which are DHP-receptor proteins with a high degree of sequence homology to the skeletal muscle DHP-receptor (Mikami et al., 1989). Cytoplasmic regions

**Present address:* Dept. Pharmacology SJ-30, University of Washington, Seattle, Washington 98195

Correspondence to: W.F. Gilly

of the cardiac molecule, however, do not interact with the SR of skeletal muscle in the Ca influx-independent way that those of the skeletal muscle protein can (Tanabe et al., 1990). To what extent Ca influx activates contraction directly *vs.* indirectly through Ca-induced Ca release from the SR (Fabiato, 1985) remains controversial and may vary between species and/or types of cardiac muscle.

Important questions remain about mechanisms involved in the final steps of E-C coupling in both skeletal and cardiac muscle, and about the roles played by charge movement, Ca channel proteins and Ca itself (Rios et al., 1990). Such focused questions can also be asked about skeletal muscle cells of invertebrates, an extremely diverse group. Here, our background knowledge is far less complete. Studies that can be most directly compared to those on vertebrates have come primarily from a few arthropod species. This phylum is the only one other than the chordata to evolve large diameter, striated muscle fibers with vertebrate-like T : SR diadic junctions (Franzini-Armstrong, 1973). Although a critical role for Ca influx through voltage-gated Ca channels has been established in both crustacean (Zachar, 1971; Atwater, Rojas & Vergara 1974; Caputo & Dipolo, 1978) and arachnid (Gilly & Scheuer, 1984) muscle fibers, it remains unknown whether Ca current directly activates the myofibrils or triggers an amplified release of Ca from the SR (Lea & Ashley, 1989) in any particular muscle fiber type of either group. This uncertainty is much like the case in vertebrate cardiac muscle.

A thorough understanding of the role in E-C coupling played by Ca channel proteins in arthropod muscle will require careful analysis of Ca currents, charge movements and intracellular Ca transients of the type exemplified by recent work on vertebrates (Hui & Chandler, 1991; Pizarro et al., 1991). The present paper examines voltage-dependent Ca and K currents that are responsible for action potential propagation and the initiation of contraction in scorpion muscle. E-C coupling relies on the influx of Ca during the repetitive action potentials in scorpion muscle (Gilly & Scheuer, 1984), and voltage-dependent charge movement in this preparation, as in vertebrate cardiac muscle, appears to gate the relevant Ca channels (Scheuer & Gilly, 1986). Characterization of the Ca currents in the scorpion muscle fiber membrane provides a basis for understanding their relationship to E-C coupling and to voltage-dependent charge movements.

Materials and Methods

All experiment used the long closer muscle of the pedipalp from *Centruroides sculpturatus*. This muscle consists of two fiber bundles connected to a common distal apodeme (Gilai & Parnas, 1970). The proximal muscle ends were left attached to a fragment of cuticle, and the preparation was pinned at 1.3 × slack length to the Sylgard-covered floor of a 35 mm tissue culture dish. Muscle fibers were visualized at 500 × total magnification through a compound microscope using a water immersion objective (Zeiss, 40 ×) and Kohler illumination. Fibers from both muscle portions were used; no systematic differences were observed. A minor population of long sarcomere fibers also exists, but this fiber type was not studied.

Current from the distal 200 μ of an individual muscle fiber was studied using the three-microelectrode voltage clamp technique (Adrian, Chandler & Hodgkin, 1970; Ashcroft & Stanfield, 1982). Electrode separations relative to the fiber end were measured with an optical micrometer. Microelectrodes were of 10–20 MΩ resistance, shielded with conductive silver paint, insulated with epoxy and nail polish, and filled with 3 M KCl or 1.5 M K-citrate as described previously (Gilly & Scheuer, 1984).

One voltage-sensing electrode, V_2, and the current-passing electrode, I, were normally inserted 200 μ from the fiber end. A second voltage electrode, V_1, was inserted midway between the V_2 site and the fiber end. Bath voltage, V_o, was held at virtual ground by a feedback circuit (Schneider & Chandler, 1976) and measured near the V_1 site by a third voltage electrode positioned just outside the fiber. Membrane voltage ($V_1 - V_o$) was fed to a voltage clamp, whose output was connected to the current-injecting microelectrode. Membrane current density around the V_1 site, $I_m(V_1)$, is approximately proportional to the voltage difference recorded by the two voltage electrodes, $\Delta V = V_1 - V_2$. The ΔV and V_1-V_o signals were amplified, filtered at 2–3 KHz with an 8-pole Bessel filter, and fed to the multiplexed input of a computer-controlled pulse generation/data acquisition system for digitization at 10 KHz.

Linear ionic and capacity (control) currents were subtracted from displayed records of voltage-dependent currents in a standard way. Control pulses were initiated at −135 mV and were of the same sign as corresponding test pulses delivered from −80 mV. Control pulses <55 mV in amplitude were the same size as the corresponding test pulses. For larger test pulses, two control pulses of 0.5 × test pulse magnitude were added together. Control currents thus generated were individually stored during the experiment and only subtracted from test pulses at the time of analysis. Test and control pulses that were poorly matched, or control pulses that showed time-dependent current, were rejected at that time. I_m in all displayed records has been normalized to the membrane capacity measured with the control pulses (Schneider & Chandler, 1976).

Compositions of bathing solutions are given in the Table. $CoCl_2$ and 3,4 diaminopyridine (di-AP) were added to achieve the final concentrations as indicated. All solutions were pH 7.0–7.2. Bath temperature was maintained at 6–12 ± 0.5°C.

Results

Figure 1 presents an overview of ionic currents which underlie regenerative electrical activity in scorpion muscle. A muscle fiber was first bathed in normal scorpion saline containing 2.5 mM Ca and current (Fig. 1*Aa*, Ca) was recorded for a voltage step to +5 mV (Fig. 1*Ab*). Upon depolarization inward current activates rapidly and then turns out-

Table. Solutions

Name	Na	K	Ca	Ba	Mg	NMG[a]	TEA	Rb	Co	Tris
(A) Normal Scorpion Saline	250	7.7	2.5	0	5	0	0	0	0	10
(B) Na-free TEA Saline [TEA] [[b]/TEA]	0	0	[b]	[b]	5[b]	0	240	7.7	[b]	10
(C) Ca-, Ba-free [[b]/Ca-free]	250	7.7	0	0	10	0	0	0	[b]	10
(D) Na-, Ca-, Ba-free [[b]/NMG]	0	7.7[c]	0	0	10	240[c]	0	0	[b]	10

[a] NMG is N-methylglucamine.

[b] The concentrations of some constituents varied with the experiment and are specified in the appropriate place by including the concentration with the name of the solution. For example, [2.5 Ca/TEA] refers to TEA saline containing 2.5 mM $Cacl_2$.

[c] When elevated KCl concentrations were used, an equivalent amount of NMGCl was omitted. For example, [125 K NMG] contains 125 mM KCl and 125 mM NMGCl.

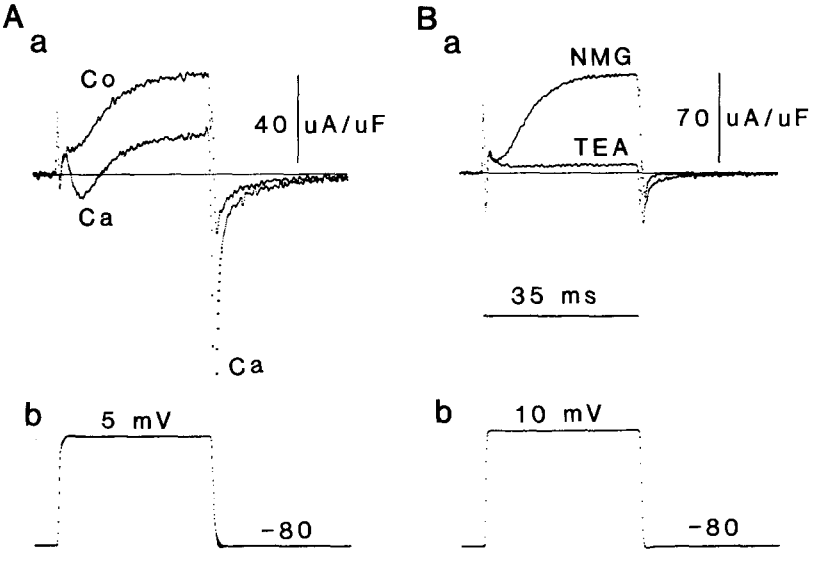

Fig. 1. Ionic currents in scorpion muscle fibers. (*A*) Ionic currents (*a*) in Normal Scorpion Saline (Ca—Solution A, Table) and after replacing Ca with 2.5 mM Co (Co—2.5 Co/Ca-free, Solution C, Table). Voltage trace is shown in (*b*). T = 13°C, fiber 14NO51. (*B*) Ionic currents (*a*) in Ca-free solution in response to voltage steps from −80 to +10 mV (*b*). Current was recorded first in a Ca-free saline containing 7.7 mM K (NMG—2.5 Co/NMG, Solution D, Table) and then in a saline with NMG replaced by TEA (TEA—2.5 Co/TEA, Solution B, Table). T = 7°C; fiber 19NO51.

ward. Following repolarization to −80 mV, a large tail of inward current flows. Replacement of Ca in the saline by Co abolishes both inward current during the pulse and the large, fast portion of the tail current (Fig. 1*Aa*, Co). Current eliminated by the exchange of Co for Ca (i.e., Co-sensitive) is the subject of the first half of this paper. It is important for both action potential propagation (Gilly & Scheuer, 1984) and contractile activation (Scheuer & Gilly, 1986).

The second half of this paper describes voltage- and time-dependent outward current recorded when inward current is blocked, e.g., by Ca-free salines containing Co. Figure 1*Ba* (NMG) shows an example of this outward current recorded in a Na- and Ca-free solution. Replacement of NMG with TEA blocks this current (Fig. 1*Ba*, TEA). Sigmoidal activation kinetics and TEA sensitivity of outward current are suggestive of delayed rectifier K currents.

The two time- and voltage-dependent currents just described are the major ones recorded from scorpion muscle under our conditions. However, when these two currents are blocked in Ca-free solutions containing isotonic TEA, a small time-independent current remains. The initial jump of current at the onset of each voltage step in Fig. 1 *Aa,Ba* and at least some of the steady current in the presence of TEA (Fig. 1*Ba*) are indicators of this third current. This "pedestal" leakage current is apparently voltage dependent, but it is generally small enough to be ignored. We have not identified the permeant ions carrying this current, but cobalt and other divalent cations reduce it (e.g., Fig. 2*Ab*). Only experiments in which voltage-dependent leakage for large voltage

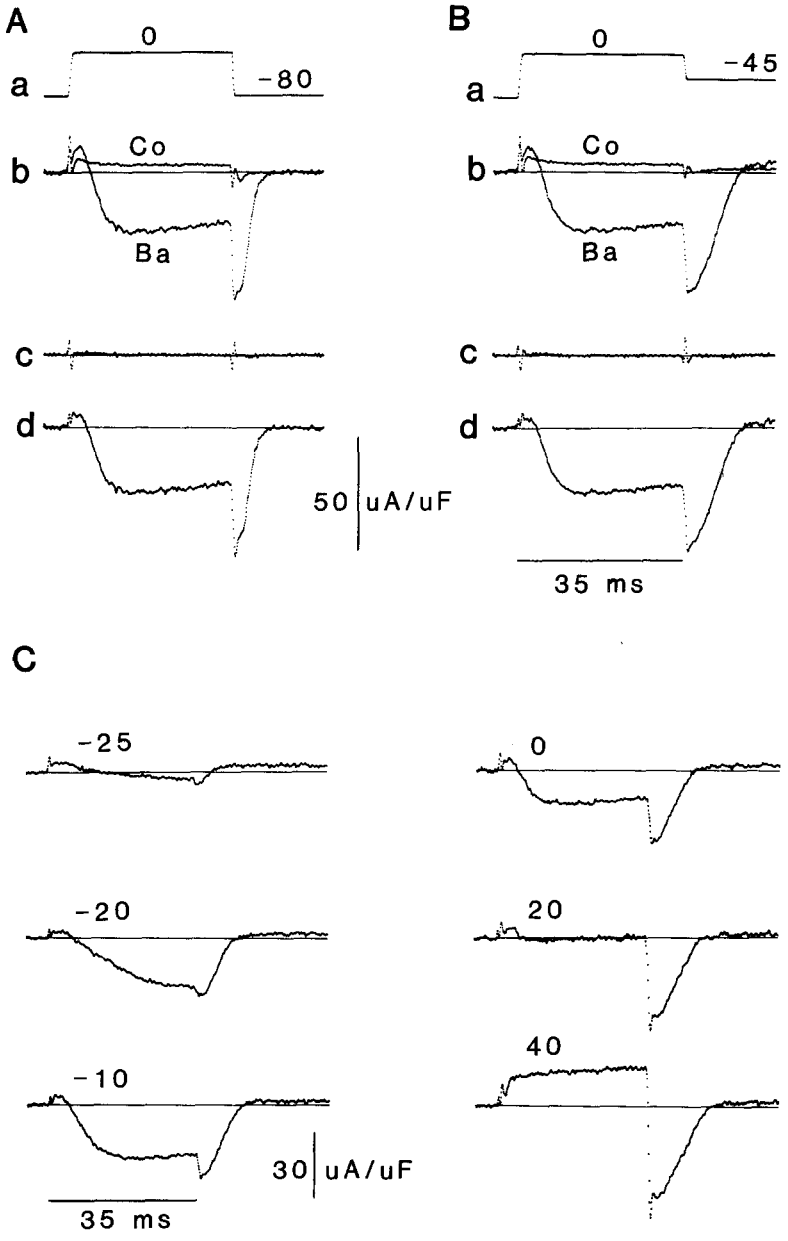

Fig. 2. Cobalt-sensitive barium current. (*A*) In the presence of 2.5 mM Ba a voltage clamp step to 0 mV (*a*) results in a large inward current (*b*, Ba) during the pulse and a large inward tail after the fiber is repolarized (2.5 Ba/TEA, Solution B, Table). Inward current is blocked (*b*, Co) when the fiber is bathed in Ba-free solution containing 5 mM Co (0 Ba + 5 Co/TEA, Solution B, Table). (*c*) Signal resulting from direct subtraction of the voltage pulses responsible for the two current traces shown in (*b*). The gain for this signal is identical to that used for the currents. (*d*) Co-sensitive current resulting from subtraction of the two traces shown in (*b*). (*B*) Barium currents elicited by the illustrated voltage steps with repolarization to −45 mV. Traces (*b*), (*c*) and (*d*) were obtained by the same procedures as the analogous traces in *A*. (*C*) A series of Co-sensitive currents was obtained at the indicated voltages by the method illustrated in Fig. 2*B*. $T = 8°C$; fiber 04DE55.

steps was small and stable over time were included in our analyses of time-dependent currents.

Ca-Channel Currents in Scorpion Muscle

Identification of Ca-Channel Current

Voltage- and time-dependent inward currents can be readily associated with Ca channels in scorpion muscle. In experiments carried out in salines containing isotonic TEA: (i) Barium (Ba) can substitute for Ca in supporting inward current; (ii) Ca (or Ba) removal eliminates inward current; (iii) Cobalt (Co) blocks this current in the presence of Ba or Ca (Scheuer & Gilly, 1986).

The amount of Ca entering a scorpion muscle fiber during voltage-clamp pulses in Ca-containing salines may be sufficient to activate contraction (Gilly & Scheuer, 1984), and the resulting twitch generates movement artifacts which distort the current waveform. Low Ca salines support measurable currents without fiber movement, and this approach was sometimes useful. Ba influx does not support contractile activation (Scheuer & Gilly, 1986), and for this reason most of our experiments used Ba ions

as the current carrier. Also, because Co effectively blocks current through scorpion Ca channels, we generally used Co-sensitive Ba currents (I_{Ba}) as a specific and reliable measure of Ca channel current.

Figure 2 illustrates examples of Co-sensitive I_{Ba} and the procedure used to generate the records. Current in response to an 80 mV depolarization (Fig. 2*Aa*) was first recorded in isotonic TEA containing 2.5 mM Ba (Fig. 2*Ab*; Ba). The solution was then changed to a Ba-free saline containing 5 mM Co, and the trace labeled Co was recorded. Inward current during the pulse and nearly all of the tail current afterward are eliminated. The remaining current in Co consists of nonlinear leakage current (which Co reduced from the control level) and voltage-dependent charge movement (which persists in Co; Scheuer & Gilly, 1986).

Direct subtraction of the traces in Fig. 2*Ab* defines Co-sensitive I_{Ba} (Fig. 2*Ad*). The initial outward jump at pulse onset is a combination of nonlinear leakage current which was blocked by Co and a smaller amount of charge movement. Figure 2*Ac* shows the subtracted voltage traces recorded with and without I_{Ba} flowing. Figure 2*B* shows analogous records for a voltage step returning to −45 mV. The Ba tail current is slower at such depolarized voltages, allowing a more reliable separation of Ba current tails from the capacity transients (*cf.* Scheuer & Gilly, 1986). Cobalt-sensitive I_{Ba} recorded in this manner over a range of activating voltages is shown in Fig. 2*C*.

Reversal Potential for Ca-Channel Current

I_{Ba} in Fig. 2*C* appears to pass through a reversal potential between +20 and +40 mV. This reversal potential can be identified by close examination of the time-dependent, Co-sensitive currents in this voltage range. In the records of Fig. 3*A* there is little net inward current at 10 mV, but the trace should be interpreted as a sizable inward current developing from a plateau of outward pedestal current. Time-dependent current at +40 mV is faster than at +10 mV, and its direction is clearly outward; at +30 mV little or no time-dependent current is present. Figure 3*B* shows records from another fiber in which a reversal potential near +30 mV can be identified. We see no sign of multiple components for time-dependent currents under these conditions, and therefore equate I_{Ba} with the time-dependent, Co-sensitive current.

Peak values of I_{Ba} from the data in Fig. 2*C* are plotted as a function of activating voltage in Fig. 4*A*. I_{Ba} first activates between −40 and −30 mV, reaches a peak near −10 mV and then declines, reversing polarity at +35 mV. This I_{Ba}-V curve is typical, and the value of reversal potential thus obtained from five fibers was in each case approximately +35 mV.

A second procedure was also followed to determine reversal potential which did not require Co subtraction. Instead, Ca channel current was selectively reduced by slow inactivation (*see also below*) at a depolarized holding potential without changing the external Ca level. This procedure should change Ca (or Ba) current both positive and negative to the actual reversal potential, but not at the reversal potential itself. Figure 4*B* shows the results of such an experiment.

Currents were first recorded in low Ca saline (1.5 mM) from a holding potential of −80 mV. Peak currents (I_{Ca} plus nonlinear leak) were directly measured, and the corresponding current-voltage curve is plotted in Fig. 4*B* (○). Holding potential was then changed to −45 mV and a matching family of currents was recorded (■). Ca current was dramatically reduced at all voltages. Finally the holding potential was returned to −80 mV to assess recovery (△). The three *I-V* curves thus cross one another between +40 and +45 mV at the actual reversal potential for the Ca-channel current in this fiber. Results from this type of analysis in another fiber yielded a value for reversal potential of +47 mV.

Ca channel current thus passes bi-directionally through the channels, and the two different methods of determining reversal potential are in good agreement. Although Ca and Ba clearly carry inward current through the Ca channels, we have not identified the permeant ion carrying outward current. Presumably it is an intracellular cation, most probably potassium.

Voltage Dependence of Calcium Channel Conductance

Two standard methods were used to determine the steady-state conductance (G)–voltage relation for Ca channels. The first method assumed that $G_{Ba} = I_{Ba}/(V - V_{Ba})$, where I_{Ba} is peak current and V_{Ba} is the reversal potential. The second method relied only on the initial amplitude of the inward tail current upon termination of each activating pulse. Because tail currents are all recorded at the same driving force, the amplitude of the tail is directly proportional to the number of channels open at the end of the activating pulse.

Barium conductance-voltage relations determined by both methods are plotted in Fig. 5*A*. Data from tail currents (○) and from currents during the pulses (■) are in good agreement and

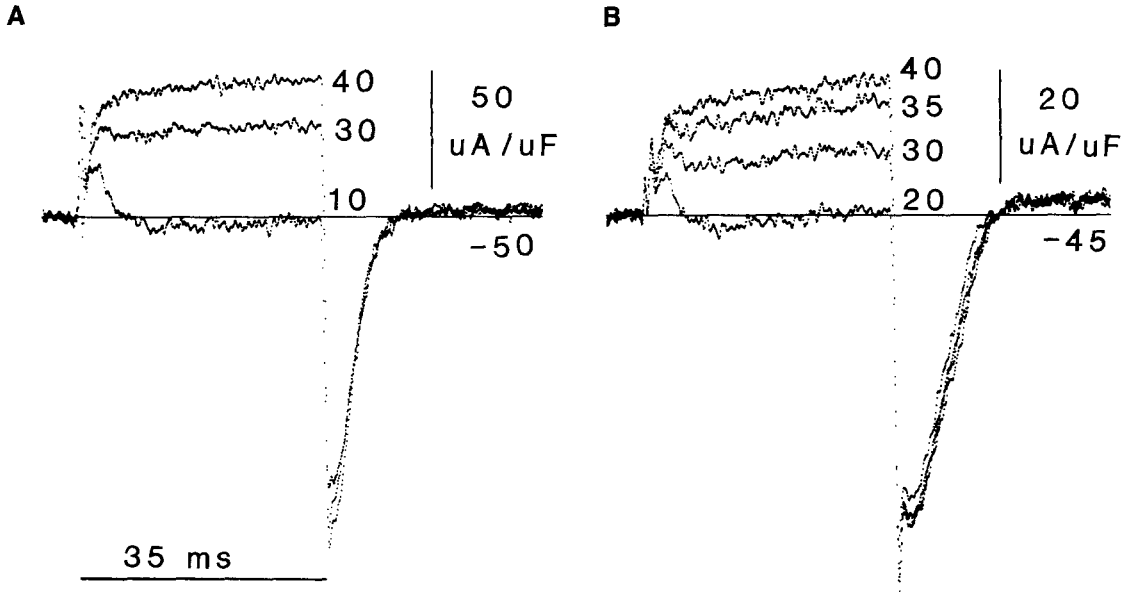

Fig. 3. I_{Ba} obtained with large activating pulses to show reversal potential. (*A*) Co-sensitive I_{Ba} for voltage pulses to +10, +30 and +40 mV are superimposed. For each pulse the repolarization potential is −50 mV. (2.5 Ba/TEA ± 5 Co/TEA; Solution B, Table). T = 9°C; fiber 03DE53. (*B*) Similar currents from another experiment with voltage pulses to +20, +30, +35 and +40 mV. Repolarization level is −45 mV. (2.5 Ba/TEA ± 5 Co/TEA; Solution B, Table). T = 8°C; fiber 04DE55.

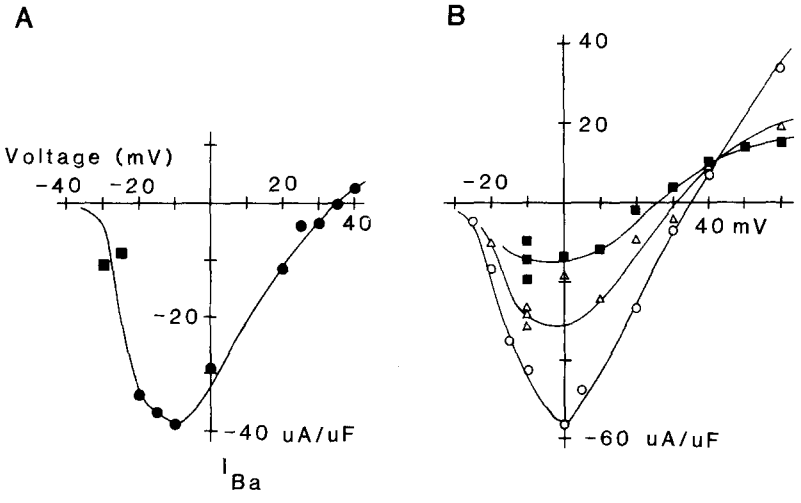

Fig. 4. Current-voltage curve for I_{Ba}. (*A*) Values of time-dependent Co-sensitive current from the experiment in Fig. 2*C* are plotted as a function of activating voltage (●). For two voltages where currents in the presence of Co were not available, values of time-dependent Ba current alone are plotted (■). (*B*) Effect of holding potential on the I_{Ca} *vs.* voltage curve. Fiber resting potential was initially set at −80 mV, and a series of depolarizing pulses was applied. Peak current recorded at each potential is plotted (○). The resting potential was then changed to −45 mV for 1 min, and the same pulse series was delivered (■). Resting potential was then returned to −80 mV for 1 min and a third series of measurements made (△). Unbroken curves were drawn by eye. (1.5 Ca/TEA; Solution B, Table); T = 7°C; fiber 23OC51.

show that G_{Ba} conductance rises steeply with voltage, reaching its half-maximal value at approximately −25 mV.

A useful measure of the steepness of the conductance-voltage relation can be made just beyond threshold for Ca channel activation (i.e., negative to −20 mV; Almers, 1978). A plot of G_{Ca} *vs.* voltage for small activating pulses is given in Fig. 5*B*; G_{Ca} increases approximately *e*-fold per 5.5 mV. Similar Ca and Ba conductance-voltage curves were determined in five fibers, and the average slope (fit by eye to the data points) was 3.99 ± 0.62 mV (mean ± SEM).

Activation Kinetics of Ca Channels

Single time constants were fit to the turn-on of I_{Ba} at different test pulse voltages and to tail currents at a series of repolarization voltages (*see* legend to Fig. 6). Opening (○) and closing (■) time constants are plotted *vs.* voltage in Fig. 6. Taken together,

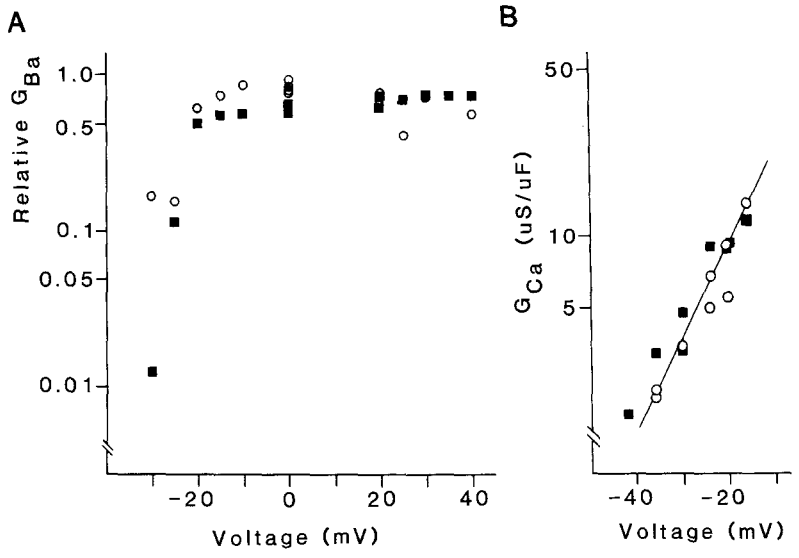

Fig. 5. Voltage dependence of Co-sensitive Ca channel conductance. (*A*) Co-sensitive I_{Ba} values from the *I-V* relation in Fig. 2*C* were converted to conductance (*G*) by the formula: $G_{Ba} = I_{Ba}/(V - V_{Ba})$, where *V* was the test pulse voltage and V_{Ba} was the measured reversal potential, +35 mV. Normalized values of G_{Ba} thus obtained are plotted as a function of test pulse potential (■). Peak tail current amplitudes recorded at −45 mV were normalized to the same maximum level and also plotted as a function of the voltage of the preceding test pulse (○). (*B*) Calcium currents measured near threshold using small test pulses. Currents (not Co-subtracted) during the pulse and current tails following the pulse were measured. Conductances, G_{Ca}, obtained during the pulse (■) and from tails (○) are plotted as a function of test pulse potential. The line through the points denotes an *e*-fold change in conductance in 5.5 mV. (1.5 Ca/TEA; Solution B, Table). T = 8°C; fiber 22NO51.

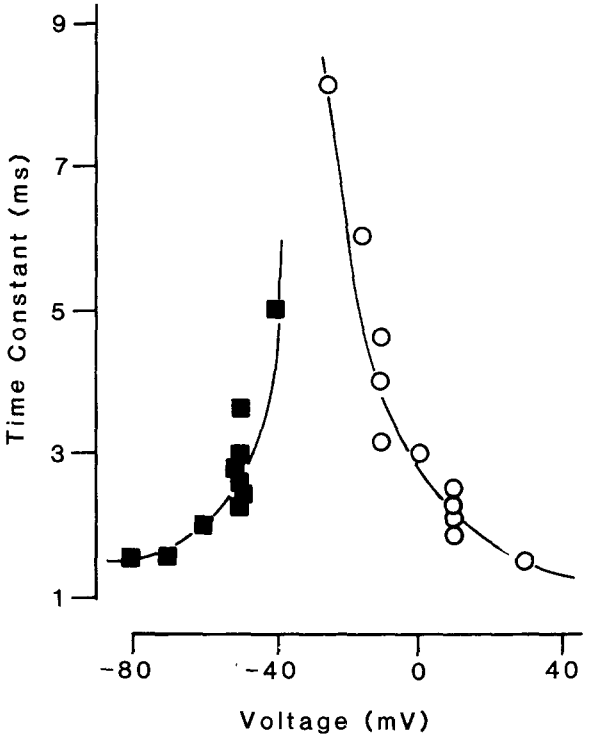

Fig. 6. Barium current kinetics. Time-constants measured for I_{Ba} activation during test pulses (○) and for deactivation measured from current tails (■) are plotted *vs.* potential. Time constants were obtained by a least-squares fit of a single exponential to the current records. Values for I_{Ba} activation were obtained by fitting the final activation time course. Current tails were readily fit to a single exponential. (2.5 Ba/TEA; Solution B,Table). T = 9°C; fiber 03DE53.

these data describe a bell-shaped curve with a sharp maximum near −20 mV, a value close to that for half-maximal activation of G_{Ba}. Limiting values at both negative and positive extremes of voltage, respectively, are undoubtedly influenced by the frequency response of our voltage-clamp method.

Fast Inactivation of Ca-Channel Current

Ba and Ca currents generally decline little during 35 msec depolarizations (*see* Figs. 2–3). The extent of this decline varies mostly from fiber to fiber and somewhat with voltage, but it does not depend dramatically on whether Ca or Ba is the permeant ion. Longer pulses do, however, reveal a phenomenon which superficially resembles voltage-dependent inactivation.

Prepulses 600 msec in duration and of variable amplitude were followed by a fixed test pulse to 0 mV in order to test for inactivation (*see inset to* Fig. 7*A*). I_{Ba} recorded at 0 mV following prepulses to +60 and −10 mV and with no prepulse (−80 mV) are illustrated in Fig. 7*A*. Inward I_{Ba} is completely eliminated by the prepulse to −10 mV, but, surprisingly, the prepulse to +60 mV potentiates the subsequent inward current relative to the control (−80 mV).

Figure 7*B* shows a more complete analysis of test pulse current (at 0 mV) *vs.* prepulse voltage. Test I_{Ba} is reduced by prepulses positive to −40 mV and is eliminated by −10 mV. For prepulses positive to 0 mV, test I_{Ba} increases. For a prepulse close to the Ca channel reversal potential, e.g., +35 mV, test I_{Ba} is approximately equal to that recorded with no prepulse at all (i.e., −80 mV). Prepulses larger than +35 mV potentiate I_{Ba}. The unbroken curve in Fig. 7*A* would thus describe "steady-state inacti-

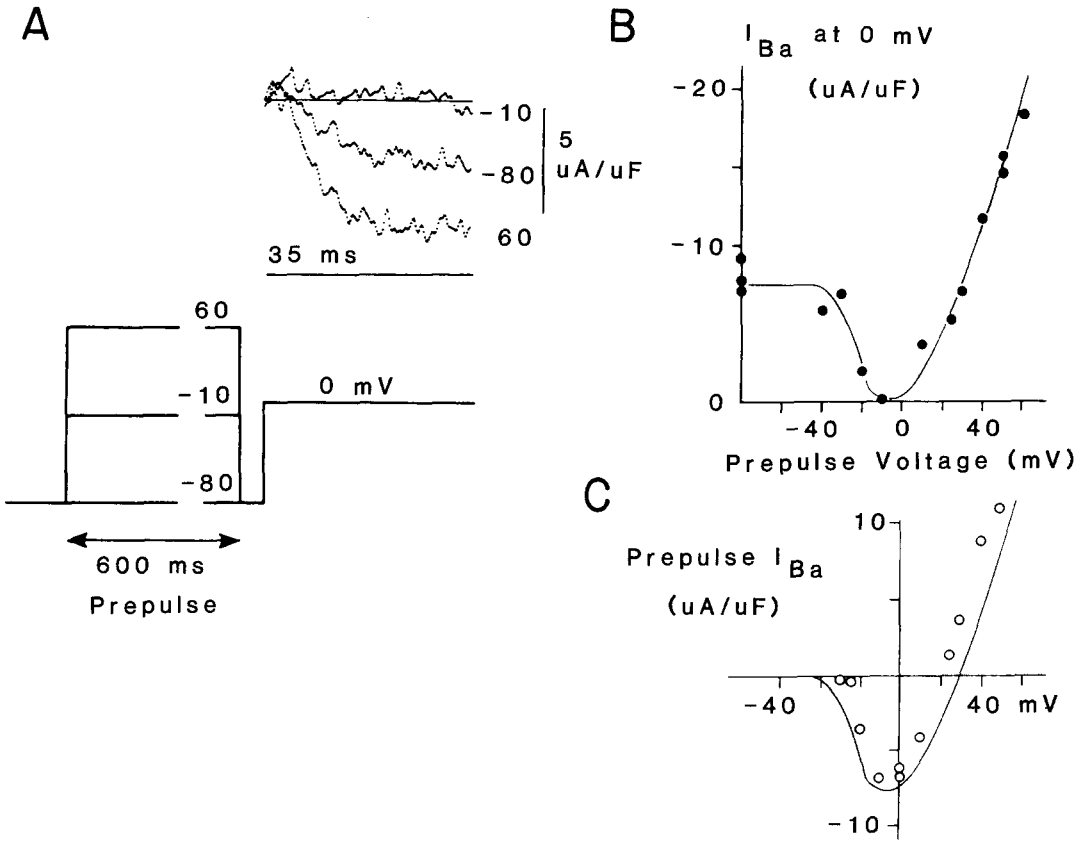

Fig. 7. Effects of depolarizing prepulses on I_{Ba}. (*A*) The voltage protocol (*see inset*) was a 600 msec prepulse to a variable potential, a 10 msec repolarization to −80 mV and finally a test pulse to 0 mV. The currents shown were measured at 0 mV following prepulses to the indicated voltages. (*B*) Peak I_{Ba} during a test pulse to 0 mV is plotted as a function of prepulse potential. (*C*) Current-voltage curve for peak I_{Ba} flowing during the initial 35 msec of the 600 msec prepulses used in (*B*). The unbroken curve through the points is the same curve as was drawn in panel *B* but here is shifted along the current axis. (2.5 Ba/TEA; Solution B, Table). T = 6°C; fiber 04DE53.

vation" for scorpion Ca channels. Although the curve negative to −10 mV would appear conventional, that positive to −10 mV requires explanation.

Peak I_{Ba} during each prepulse in the experiment of Fig. 7*B* was also measured, and these data are plotted as a function of voltage in Figure 7*C* (○). This prepulse current-voltage curve overlaps with the "steady-state inactivation" curve that is redrawn in Fig. 7*C* (unbroken curve) after a downward shift on the current axis so that I_{Ba} at −80 mV in Fig. 7*B* equals zero in Fig. 7*C*.

The close match of these activation and inactivation curves for both inward and outward Ca-channel currents strongly suggests that a current-dependent mechanism is responsible for both the prepulse-induced inactivation and potentiation. At this point we tentatively conclude that depletion of Ca in the TT system is responsible for the "inactivation" seen negative to −10 mV (Almers, Fink & Palade, 1981). Furthermore, we suggest that accumulation of the intracellular cation that carries outward current through the channel underlies the potentiation seen with prepulses positive to the reversal potential. Although this explanation might not apply to vertebrate Ca channels that permit a significant influx of monovalent cations only in the absence of external calcium (Almers, McCleskey & Palade, 1984; Hess & Tsien, 1984), the Ca channels in scorpion muscle may differ in this regard (*cf.* Scheuer & Gilly, 1986). This question merits further investigation.

Slow Inactivation of Ca Channels

Slow inactivation induced by depolarized holding potentials as demonstrated in Fig. 4*B* clearly differs from the much faster current-dependent inactivation just described. Prepulses, as used above between

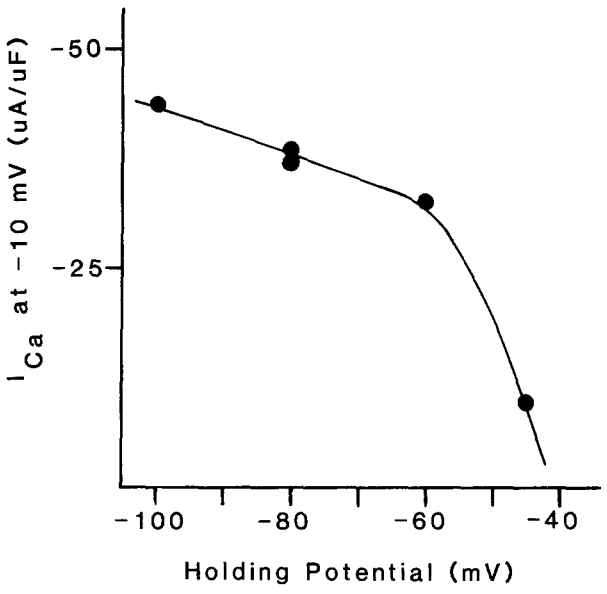

Fig. 8. Slow inactivation of G_{Ca}. I_{Ca} was measured with a test pulse to +10 mV from a series of holding potentials. Each holding potential was maintained for 1 min. I_{Ca} amplitude is plotted as a function of holding potential. Holding potential was changed in the following order: −80, −100, −80, −60, −45 mV. Recovery at −80 mV following this series was only 50% complete (*datum not illustrated*). (2 Ca/TEA; Solution B, Table). T = 8°C; fiber 15OC55.

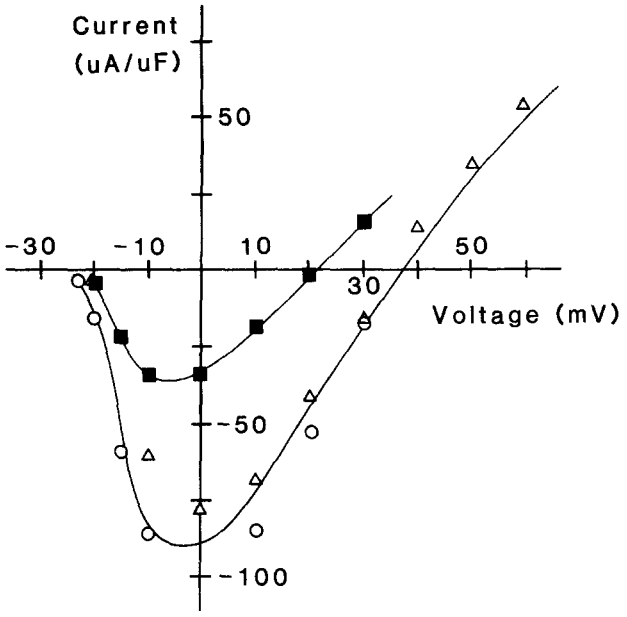

Fig. 9. Current-voltage curves in Ca- *vs.* Ba-containing solutions. Peak time-dependent currents were measured during pulses to a series of voltages in a solution containing 2 mM Ca (○). The solution was then changed to one containing 2 mM Ba and the pulses were repeated (■). A final bracketing run was then taken in 2 mM Ca (△). (2 Ca *vs.* 2 Ba/TEA; Solution B, Table). T = 8°C; fiber 18OC51.

−80 and −40 mV, produce almost no detectable inactivation (or activation) of I_{Ba}, but changing the holding potential over this range produces a strong effect on the maximal amount of I_{Ba} which can be activated by a strong test pulse (*see* Fig. 8).

Slow inactivation occurred with either Ca or Ba as the current carrier and thus appears to be primarily voltage dependent. The resting potential of scorpion muscle fibers is approximately −70 mV (Gilly & Scheuer, 1984), and most of the Ca channels would thus be available for action potential generation. Slow inactivation was not completely reversible after depolarizations positive to −50 mV, and therefore it was not studied in detail.

Calcium Channel Selectivity: Ca vs. Ba

Ca and Ba do not pass through scorpion Ca channels with equal ease. Figure 9 shows current-voltage relations from a fiber obtained in 2 mM Ca (○), in 2 mM Ba (■), and following return to 2 mM Ca (△). A similar reduction in peak current in changing from Ca to Ba (on an equimolar basis) was found in every fiber thus studied. Conductance for outward current through the Ca channel does not depend on whether Ca or Ba is present extracellularly.

Outward Current in Scorpion Muscle

Voltage-Dependence of TEA-Sensitive Current

TEA-sensitive currents were generated by subtraction of records taken before and after total Na (or NMG) replacement with TEA (e.g., Fig. 1*B*). Figure 10*A* shows a family of such currents. Similar voltage- and time-dependent outward currents were also recorded directly (without a solution change) in Ca-free solutions containing 2–5 mM Co (*see* Fig. 10*B*). TEA-sensitive currents resemble the currents recorded in Ca-free, Co-containing solutions, but generally show a smaller pedestal of voltage-dependent leak current.

Time-dependent outward currents are first apparent near −25 mV and grow steadily with increasing depolarization. Their time course is characterized by a pronounced initial delay. This delay shortens and activation kinetics become faster as voltage becomes more positive. Inward current tails upon repolarization are slow, even at −80 mV (Fig. 10*B*). Voltage dependence of peak outward

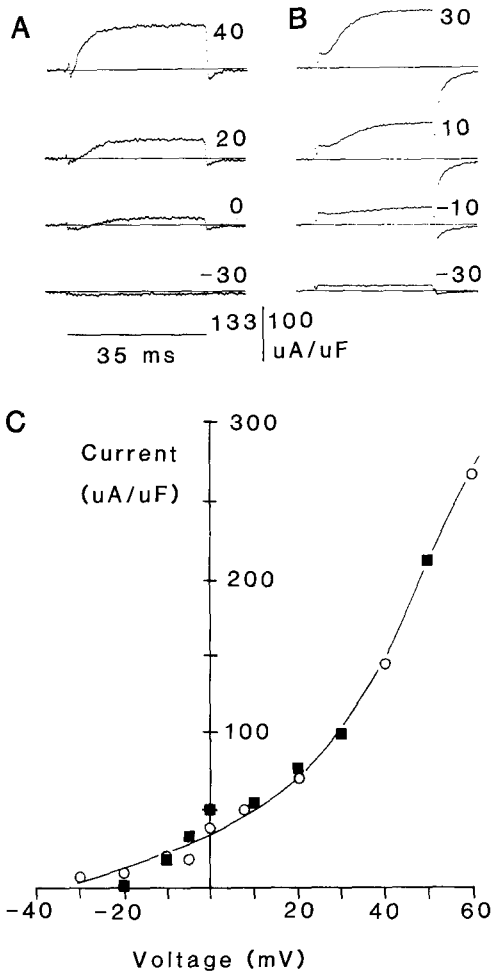

Fig. 10. Voltage- and time-dependent outward currents. (*A*) TEA-sensitive outward currents. Currents were first recorded during pulses from −80 mV to the indicated voltages in a Ca-free saline (0 Co/Ca-Free; Solution C, Table). Repolarization level following each pulse was −45 mV. Na in the solution was then replaced with TEA (0 Ca, 0 Co/TEA; Solution B, Table), and the same voltage pulses were repeated. The illustrated records were generated by subtracting the paired currents. T = 6°C; fiber 13NO52. (*B*) Outward currents recorded in the presence of cobalt for pulses from −80 mV to the indicated voltages (2.5 Co/NMG saline, Solution D, Table). Repolarization level after each pulse was −80 mV. T = 7°C; fiber 14NO52. (*C*) Values of TEA-sensitive current from *A* are plotted as a function of voltage (○). Currents displayed in *B* have been scaled by a factor of 0.57 for comparison (■). This scaling factor was chosen to match time-dependent current amplitudes at +30 mV in the two experiments.

current, measured from the pedestal current level in these experiments, is illustrated in Fig. 10*C*.

Dependence of the Outward Current on Potassium Ions

Selectivity of the outward current for potassium ions was assessed by determining the reversal potential in Co-containing NMG solutions (Solution D, Table) containing either 7.7 or 125 mM K ($[K_o]$). Examples of records obtained in 125 mM K are illustrated in Fig. 11*A*. Reversal potential was more positive at elevated $[K_o]$, the values being −33 ± 4.5 mV in 7.7 mM K *vs.* −4.5 ± 3.5 mV in 125 mM K (N = 4 at each concentration). This change in reversal potential (24 mV per 10-fold change in $[K_o]$) is less than that predicted for perfect K selectivity. The discrepancy may reflect accumulation of K ions in the lumen of transverse tubules in the low K solution but not in high K. Other factors may also be important. No attempt was made to investigate selectivity of this channel which carries K and is blocked by TEA in any greater detail.

Voltage Dependence of G_K

Total K conductance, G_K, was estimated from the amplitude of the inward tail current following an activating pulse to a particular voltage. In order to increase the amplitude of tail currents and to minimize effects of K accumulation or depletion in any restricted spaces, these experiments were carried out in high $[K_o]$ (*see* Fig. 11*A*). G_K attained at the end of each activating pulse was calculated from the peak tail current amplitude and a driving force of −75 mV (K channel reversal potential = −5 mV). The resulting $G_K - V$ relation is plotted in Fig. 11*B* and has a limiting slope over the most negative voltages equal to an e-fold change in G_K per 7 mV. $G_K - V$ relations thus recorded from four different fibers gave an average maximum steepness of an e-fold G_K change in 9.9 ± 0.83 mV (mean ± SEM). In one experiment $G_V - V$ relationships were determined in both 7.7 and 125 K, and the steepness was not significantly altered.

I_K Activation Displays a Pronounced Voltage-Dependent Delay

One characteristic of delayed rectifier I_K in many nerve and muscle cells is that the delay in I_K activation can be greatly prolonged if the test pulse is preceded by a strong hyperpolarization (Cole & Moore, 1960). Such a protocol applied to scorpion muscle produces this result. A test depolarization to +30 mV was applied either with or without a 200 msec hyperpolarizing prepulse from −80 to −135 mV, and the resulting traces in Fig. 12*A* reveal a pronounced delay in the onset of I_K due to the prepulse. Ca channel currents in scorpion muscle do not share this kinetic feature (*data not illustrated*).

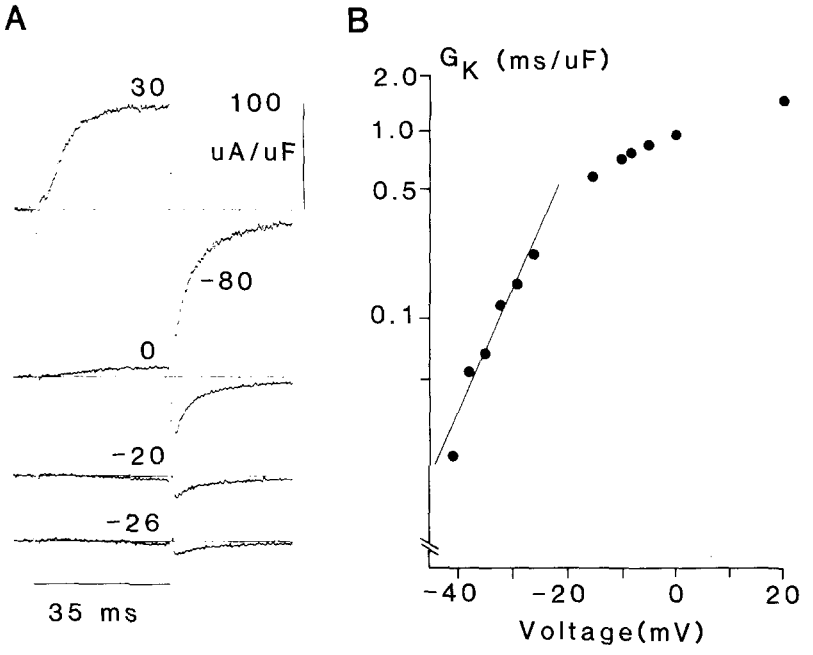

Fig. 11. Voltage dependence of potassium conductance. (*A*) Currents recorded in high external K at the indicated voltages (125 K, 2.5 Co/NMG; Solution D, Table). (*B*) G_K-voltage curve is obtained from the data in *A* by plotting peak I_K tail amplitude as a function of activating voltage. Tail magnitudes were measured with reference to the final current level at the end of the trace. T = 6°C; fiber 21NO53.

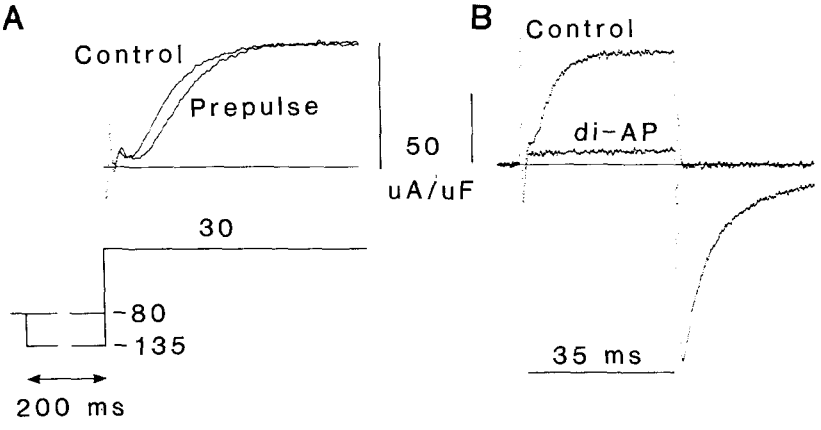

Fig. 12. Kinetic and pharmacological features of G_K activation. (*A*) Hyperpolarization-induced slowing of outward current. The outward currents shown were measured at +30 mV without (*Control*) or with (*Prepulse*) a previous 200 msec long hyperpolarization to −135 mV. (2.5 Co/NMG; Solution D, Table). T = 7°C; fiber 14NO53. (*B*) G_K block by 3,4 diaminopyridine (di-AP). I_K was recorded at +40 mV in the absence (*Control*) and presence (*di-AP*) of 0.5 mM 3,4 di-AP. (125 K, 2.5 Co/NMG; Solution D, Table). T = 8°C; fiber 21NO55.

I_K Is Blocked by 3,4 Diaminopyridine

TEA-sensitive I_K in scorpion muscle is also blocked by diaminopyridine, another common K channel blocker. Figure 12*B* illustrates the effect of 0.5 mM di-AP on I_K recorded in the presence of 125 mM K. Both outward I_K during the pulse to +40 mV and the tail at −80 mV following repolarization are completely blocked. Ca channels are not blocked in this way by di-AP (*data not illustrated*).

Discussion

This paper characterizes the voltage-dependent conductances in scorpion muscle fibers responsible for action potential generation (Gilly & Scheuer, 1984) and for E-C coupling (Scheuer & Gilly, 1986). Inward current flows through Ca channels and outward current flows through K channels. The properties of G_{Ca} and G_K presented here reinforce the previous identification of voltage-dependent charge movement in scorpion muscle as largely Ca channel gating current (Scheuer & Gilly, 1986). Steady-state voltage dependence and kinetics of charge movement match those of G_{Ca} very closely and are distinct from those of G_K. Furthermore, charge movement and G_{Ca} are not blocked by di-AP, whereas G_K is totally eliminated. Charge movement also appears to be sensitive to a slow inactivation process over a voltage range similar to that shown by G_{Ca} (*unpublished data*). Although K channel gating currents undoubtedly also exist in scorpion muscle, they are evidently too slow and small to be detectable.

All data included in this paper were obtained in recordings made at the ends of muscle fibers, and sodium (Na)-dependent or tetrodotoxin (TTX)-sensitive currents were not encountered. Thus, functional Na channels do not appear to be present over the terminal 250 μ length of muscle fiber. Whether Na channels are present elsewhere on the muscle fiber remains unknown. In vertebrate muscle Na channel density falls off dramatically at the fiber ends (Caldwell, Campbell & Beam, 1986), and a similar situation might exist in the scorpion. Alternatively, there may be no Na channels at all in scorpion muscle. Previously, we had reported that all-or-nothing twitches of scorpion muscle fiber bundles were both Na-dependent and TTX-sensitive (Gilly & Scheuer, 1984), but this may have been due to stimulation of large motor axons by the extracellular shocks used in these early experiments.

In work described here no obvious signs of multiple Ca or K conductances were found based on kinetic or pharmacological analysis. Ca channels appear to be of single type that activate rapidly at moderately positive voltages, close quickly on repolarization, and do not inactivate during a 35 msec pulse. The steady-state voltage dependence is very steep. These properties would ally scorpion Ca channels most closely with the L- (Nowycky, Fox & Tsien, 1985) or FD- (Matteson & Armstrong, 1986) type channels found in many vertebrate cell types, especially cardiac muscle (Bean, 1989). Kinetics of this type of Ca channel in vertebrate skeletal muscle is extremely slow, and even the fast I_{Ca} in frog muscle (Cota & Stefani, 1986) is slower than scorpion I_{Ca}. In comparison to I_{Ca} in other arthropod muscle types, that in scorpion is distinguished by its higher density and faster kinetics (Keynes et al., 1973; Hencek & Zachar, 1977; Ashcroft & Stanfield, 1982). Unlike action potentials in scorpion muscle which are all-or-nothing (Gilly & Scheuer, 1984), action potentials in these other arthropods are normally "graded" with stimulus intensity.

DHP-sensitivity is a defining feature of vertebrate L-type Ca channels in muscle cells, but sensitivity of scorpion Ca channels to DHP and other organic Ca channel blockers is unknown. Preliminary biochemical evidence in crayfish muscle has suggested that a DHP-receptor/Ca channel protein is present in this arthropod (Krizanova, Novotova & Zachar, 1990). Another intriguing parallel between vertebrate and arthropod muscle exists in that Ca channel activity in both groups can be modulated by neurotransmitters (Bean, 1989; Bishop, Krouse & Wine, 1991). Nothing is known about scorpion muscle in this regard.

The pathway for outward current described here in the scorpion is dominated by a voltage-dependent G_K that activates with a pronounced delay and is sensitive to the blocking compounds TEA and di-AP. I_K does not appreciably inactivate during pulses several hundred msec long. Under the conditions of our studies (no external Ca), we find no clear sign of multiple K conductances such as the voltage- or Ca-activated transient outward currents that are present in other arthropod muscle types (primarily insect—Ashcroft & Stanfield, 1982; Salkoff & Wyman, 1983; Solc, Zagotta & Aldrich, 1987).

The "normal" action potential in scorpion muscle is a repetitive discharge of brief spikes arising from a plateau voltage ~ -25 mV. The discharge lasts for the duration of the twitch (typically 100–200 msec), and its exact pattern is highly variable (*cf.* Fig. 1 in Gilly & Scheuer, 1984). This complex electrical behavior must be primarily generated by interplay of the voltage- and time-dependent G_{Ca} and G_K described here, but several secondary factors are probably also important. Although the voltage-dependent leak current in these fibers is relatively small, its apparent properties could make it a significant factor in setting threshold and in stabilizing the plateau voltage from which the oscillatory action potentials arise. Furthermore, depletion of Ca in the T-system during the episode of repetitive firing might partially "inactivate" I_{Ca} and thereby play a physiological role in termination of the action potential burst and twitch.

This work was supported by a grant from the NIH (NS-17510) to W.F.G. and a NRSA award to T.S. (GM-09921).

References

Adams, B.A., Beam, K.G. 1990. Muscular dysgenesis in mice: a model system for studying excitation-contraction coupling. *FASEB J* **4**:2809–2816

Adams, B.A., Tanabe, T., Mikami, A., Numa, S., Beam K.G. 1990. Intramembrane charge movement restored in dysgenic skeletal muscle by injection of dihydropyridine receptor cDNAs. *Nature* **346**:569–572

Adrian, R.H., Chandler, W.K., Hodgkin, A.L. 1970. Voltage clamp experiments in striated muscle fibres. *J. Physiol.* **208**:607–644

Almers, W. 1978. Gating currents and charge movements in excitable membranes. *Rev. Physiol. Biochem. Pharmacol.* **82**:96–190

Almers, W., Fink, R., Palade, P. 1981. Calcium depletion in frog muscle tubules: the decline of calcium current under maintained depolarization. *J. Physiol.* **312**:177–207

Almers, W., McCleskey, E.W., Palade, P. 1984. A non-selective cation conductance in frog muscle membrane blocked by micromolar external calcium ions. *J. Physiol.* **353**:565–583

Aschcroft, F.M., Stanfield, P.R. 1982. Calcium and potassium currents in muscle fibres of an insect (*Carausius morosus*). *J. Physiol.* **323**:93–115

Atwater, I., Rojas, E., Vergara, J. 1974. Calcium influxes and

tension in perfused single barnacle muscle fibers under membrane potential control. *J. Physiol.* **243**:583–611

Bean, B.P. 1989. Classes of calcium channels in vertebrate cells. *Annu. Rev. Physiol.* **51**:367–384

Bishop, C.A., Krouse, M.E., Wine, J.J. 1991. Peptide cotransmitter potentiates calcium channel activity in crayfish skeletal muscle. *J. Neurosci.* **11**:269–276

Caldwell, J.H., Campbell, D.T., Beam, K.G. 1986. Na channel distribution in vertebrate skeletal muscle. *J. Gen. Physiol.* **87**:907–932

Caputo, C., Dipolo, R. 1978. Contractile phenomena in voltage clamped barnacle muscle. *J. Gen. Physiol.* **71**:467–488

Cole, K.S., Moore, J.W. 1960. Potassium ion current in the squid giant axon: dynamic characteristic. *Biophys. J.* **1**:1–14

Cota, G., Stefani, E. 1986. A fast-activated inward calcium current in twitch muscle fibres of the frog (*Rana montezume*). *J. Physiol.* **370**:151–163

Fabiato, A. 1985. Time and calcium dependence of activation and inactivation of Ca-induced release of Ca from the SR of a skinned cardiac Purkinje cell. *J. Gen. Physiol.* **85**:247–289

Ferguson, D., Schwartz, W., Franzini-Armstrong, C. 1984. Subunit structure of junctional feet in triads of skeletal muscle: A freeze-drying, rotary shadow study. *J. Cell Biol.* **99**:1735–1742

Franzini-Armstrong, C. 1973. Membranous systems in muscle fibers. *In*: The Structure and Function of Muscle. Second edition, pp. 531–619. G.H. Bourne, editor. Academic, New York

Gilai, A., Parnas, I. 1970. Neuromuscular physiology of the closer muscles in the pedipalp of the scorpion *Leiurus quinquestriatus*. *J. Exp. Biol.* **52**:325–344

Gilly, W.F., Scheuer, T. 1984. Contractile activation in scorpion striated muscle fibers. Dependence on voltage and external calcium. *J. Gen. Physiol.* **84**:321–345

Hess, P., Tsien, R.W. 1984. Mechanism of ion permeation through calcium channels. *Nature* **309**:453–456

Hencek, M., Zachar, J. 1977. Calcium currents and conductances in the muscle membrane of the crayfish. *J. Physiol.* **268**:51–71

Hui, C.S., Chandler, W.K. 1991. Q_β and Q_γ components of intramembranous charge movement in frog cut twitch fibers. *J. Gen. Physiol.* **98**:429–464

Keynes, R.D., Rojas, E., Taylor, R.E., Vergara, J. 1973. Calcium and potassium systems of a giant barnacle muscle fibre under membrane potential control. *J. Physiol.* **229**:409–455

Krizanova, O., Novotova, M., Zachar, J. 1990. Characterization of DHP binding protein in crayfish striated muscle. *FEBS Lett.* **267**:311–315

Lea, T.J., Ashley, C.C. 1989. Ca-induced Ca release from the sarcoplasmic reticulum of isolated myofibrillar bundles of barnacle muscle fibres. *Pfluegers Arch.* **413**:401–406

Matteson, D.R., Armstrong, C.M. 1986. Properties of two types of calcium channels in clonal pituitary cells. *J. Gen. Physiol.* **87**:161–182

McClesky, E.W. 1985. Calcium channels and intracellular calcium release are pharmacologically different in frog skeletal muscle. *J. Physiol.* **361**:231–249

Mikami, A., Imoto, K., Tanabe, T., Niidome, T., Mori, Y., Takeshima, H., Narumiya, S., Numa, S. 1989. Primary structure and functional expression of the cardiac dihydropyridine-sensitive calcium channel. *Nature* **340**:230–233

Morad, M., Goldman, Y.E., Trentham, D.R. 1983. Rapid photochemical inactivation of Ca antagonists shows that Ca entry directly activates contraction in frog heart. *Nature* **304**:635–638

Nowycky, M., Fox, A.P., Tsien, R.W. 1985. Three types of neuronal calcium channel with different calcium agonist sensitivity. *Nature* **316**:440–443

Pizarro, G., Csernoch, L., Uribe, I., Rodriguez, M., Rios, E. 1991. The relationship between Qγ and Ca release from the sarcoplasmic reticulum in skeletal muscle. *J. Gen. Physiol.* **97**:913–947

Rios, E., Brum, G. 1987. Involvement of dihydropyridine receptors in excitation-contraction coupling in skeletal muscle. *Nature* **325**:717–720

Rios, E., Fitts, R., Uribe, I., Pizarro, G., Brum, G. 1990. A third role for calcium in excitation-contraction coupling. *In*: Transduction in Biological Systems. C. Hidalgo, editor. pp. 385–399. Plenum, New York

Rios, E., Ma, J., Gonzalez, A. 1991. The mechanical hypothesis of excitation-contraction (EC) coupling in skeletal muscle. *J. Muscle Res. Cell Motil.* **12**:127–135

Salkoff, L.B., Wyman, R.J. 1983. Ion currents in *Drosophila* flight muscles. *J. Physiol.* **337**:687–709

Scheuer, T., Gilly, W.F. 1986. Charge movement and depolarization-contraction coupling in arthropod vs. vertebrate skeletal muscle. *Proc. Natl. Acad. Sci. USA* **83**:8799–8803

Schneider, M.F. 1981. Membrane charge movement and depolarization-contraction coupling. *Annu. Rev. Physiol.* **43**:507–517

Schneider, M.F., Chandler, W.K. 1973. Voltage-dependent charge movement in skeletal muscle: a possible step in excitation-contraction coupling. *Nature* **242**:244–246

Schneider, M.F., Chandler, W.K. 1976. Effects of membrane potential on the capacitance of skeletal muscle fibers. *J. Gen. Physiol.* **67**:125–163

Shirokov, R., Levis, R., Shirokova, N., Rios, E. 1992. Two classes of gating current from L-type Ca channels in guinea pig ventricular myocytes. *J. Gen. Physiol.* **99**:863–895

Solc, C.K., Zagotta, W.N., Aldrich, R.W. 1987. Single-channel and genetic analyses reveal two distinct A-type potassium channels in *Drosophila*. *Science* **236**:1094–1098

Tanabe, T., Beam, K.G., Powell, J.A., Numa, S. 1988. Restoration of excitation-contraction coupling and slow calcium current in dysgenic myotubes by dihydropyridine receptor complementary DNA. *Nature* **336**:134–139

Tanabe, T., Beam, K.G., Adams, B.A., Niidome, T., Numa, S. 1990. Regions of the skeletal muscle dihydropyridine receptor critical for excitation-contraction coupling. *Nature* **346**:567–569

Zachar, J. 1971. Electrogenesis and Contractility in Skeletal Muscle Cells. University Press, Baltimore, MD